

The morphology and mechanical properties of PP/EPDM/nano-CaCO₃ composites: effect of initial mixing state

Lei Gong · Bo Yin · Lan-peng Li · Ming-bo Yang ·
Bang-hu Xie · Jian-min Feng

Received: 26 January 2013 / Revised: 4 June 2013 / Accepted: 6 July 2013 /
Published online: 23 July 2013
© Springer-Verlag Berlin Heidelberg 2013

Abstract Polypropylene (PP) was blended with ethylene–propylene–diene terpolymer (EPDM) and calcium carbonate nanoparticles (nano-CaCO₃), where all the components were in different initial mixing states, i.e., all in solid (solid blending composite), nano-CaCO₃ and EPDM first forming solid master batch, then being mixed with solid PP (master batch blend composite) and all in melt (melt blending composite). The phase morphology, especially the distribution of nano-CaCO₃, and mechanical properties of the resultant composites and their dependence on the initial mixing states of the components were studied systematically. Morphological observation revealed that essentially different from the respectively dispersed morphology of nano-CaCO₃ particles and EPDM phase in the PP matrix in the solid blending composite, abundant well-dispersed nano-CaCO₃ particles concentrating around EPDM phase in the melt blending composite. Due to the cavitation initiated by the debonding and the fibrillation present at interface as a result of well-dispersed nano-CaCO₃ particles, its impact strength was pronouncedly enhanced, increasing 280 % compared to PP/EPDM composite. Our work paves the way to obtain high-performance PP composites.

Keywords Processing sequence · Lateral injection extrusion · Morphology · Mechanical properties · PP · Nano-CaCO₃

L. Gong · B. Yin (✉) · L. Li · M. Yang (✉) · B. Xie · J. Feng
College of Polymer Science and Engineering, State Key Laboratory of Polymer Materials
Engineering, Sichuan University, Chengdu 610065, Sichuan, People's Republic of China
e-mail: yinbo@scu.edu.cn

M. Yang
e-mail: yangmb@scu.edu.cn

Introduction

Toughening of polypropylene (PP) has attracted much attention because PP exhibits very low impact toughness, especially at lower temperatures, which restricts its extensive applications [1–4]. Many methods have been developed to toughen PP, including copolymerizing propylene with other olefin monomers [5], blending PP with rubber or thermoplastic elastomer [6], compounding PP with organic or inorganic fillers (e.g., nanoparticles) [7, 8], introduction of β -nucleating agents [9, 10] and even submicrometer voids [11]. Except for the very limited reports on the simultaneous improvement of toughness and stiffness [11–14], the toughness of the modified PP can be enhanced effectively [5–10], but the stiffness dramatically drops compared to the pristine polymer.

The mechanical properties of the modified PP strongly depends on the morphologies, such as the crystal structures, the distribution of the dispersed phase or fillers, etc. For example, it has been well established that oriented crystals (i.e., shish-kebabs) can notably reinforce PP [15, 16], while β -form crystals of PP can greatly increase its toughness [9, 10, 17, 18]. For elastomer toughening PP systems, small particles take effect by shear yielding, whereas large particles are more effective when multiple crazing dominates by means of energy absorption [19]. Though many reports focused on the relationship between the phase morphology and mechanical properties of filled PP blends [20–23], it is still unclear. Yang et al. [24] has discovered that the filler-network structure, wherein a large amount of SiO_2 particles around ethylene–propylene–diene terpolymer (EPDM) particles and pervading over the PP matrix, could bring a simultaneous enhancement of toughness and modulus of PP. Ma and co-workers [25] have shown that both the segregated dispersion state and core–shell structure, in which ethylene–octene copolymer (POE) acted as the shell part encapsulating calcium carbonate nanoparticles (nano- CaCO_3), in the PP/POE/ CaCO_3 ternary composites could significantly increase the notched impact toughness, in comparison with PP/POE blend or neat PP; meanwhile, the stiffness and tensile strength were almost unchanged or slightly enhanced. In contrast, many study reported that nanofillers do not considerably improve the tensile mechanical properties of filled blends like the elongation and stress at break. Moreover, the impact properties of the filled blends are often reduced [26–29].

To achieve the balanced combination of mechanical properties, controlling the phase morphology of the filled PP blends, and the distribution and dispersion of the fillers, is feasible. It is well known that the final phase morphology of ternary blend is determined not only by the thermodynamic factors (e.g., interfacial tension [24, 30]), but also by the kinetic factors (e.g., shear stress and processing sequence). Up to now, the influence of kinetic factor on the phase morphology and properties for the filled PP blends has been researched extensively [31, 32], but few attention has been paid to the effect of the initial mixing state of the compositions.

In our previous paper [33, 34], we have found that, the lateral injection extrusion method can efficiently hinder the migration of the nano- CaCO_3 particles from EPDM phase to PP matrix, so that more nano- CaCO_3 particles are retained in EPDM phase or at the interface between EPDM phase and PP matrix, in comparison

with other extrusion methods like direct extrusion and two-step extrusion. In other words, lateral injection extrusion method gives rise to a special morphology in ternary composite, where the nano- CaCO_3 particles preferentially exist in EPDM phase or at the interface between EPDM phase and PP matrix. It occurs to us what effect such a special morphology will endow in the ternary composites, especially the mechanical properties? In this paper, we report our efforts to reveal the influence of the initial mixing state of the compositions, including solid, master and melt, on the distribution of CaCO_3 and mechanical properties for PP/EPDM/nano- CaCO_3 composite. Furthermore, the relationship between the microstructure and toughness of PP/EPDM/nano- CaCO_3 composite was further investigated, on the basis of the deformation mechanism during impact process.

Experimental section

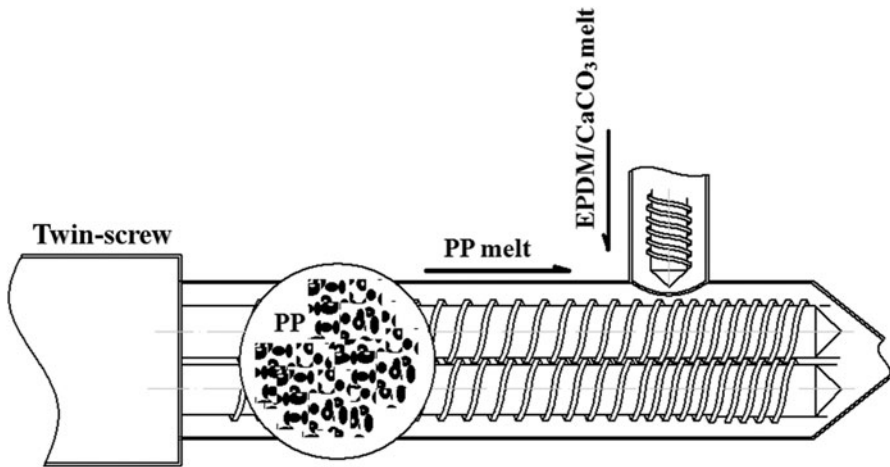
Materials

Polypropylene (PP, T30S) was purchased from Lanzhou Petrochemical Company, Ltd, China. It has a melt flow rate (MFR) of 2.6 g/10 min according to ASTM D1238.79, and a density of 0.91 g/cm³ according to ASTM D1505-68. Ethylene–propylene–diene terpolymer (EPDM) (Nordel 4725p) was purchased from Dupont Dow Elastomers L.L.C., USA. It contains 70 % ethylene, 25 % propylene and 4.9 % ENB (ethylidene norbornene), with the M_w of 135,000 g/mol. Nano- CaCO_3 particles (10–40 nm particle size) were obtained from Huaxin Nanomaterial Co. Ltd, China. The nano- CaCO_3 particles were treated by stearic acid by the manufacturer.

Sample preparation

The blend of PP/EPDM (80 w/20 w) with various content of nano- CaCO_3 (0, 4, 6 phr) were prepared. According to the mixing states of the components, the blending process for the PP/EPDM/ CaCO_3 blend was distinguished into solid blending, master batch blending and melt blending as shown in Scheme 1. Solid blending was mixed all three solid materials together at the beginning of extruding. In master batch blending, nano- CaCO_3 particles were firstly dispersed in EPDM using a mild blending method [35], then the product considered as master batch was further blended with solid PP in twin-screw extruder. The melt blending was completed via the innovative lateral injection extrusion, in which the melted master batch mentioned above in a single screw extruder blended with melted PP in twin-screw extruder via injecting into the twin-screw extruder from a lateral port at the melting section of the twin-screw extruder (Scheme 1). The processing temperature profiles in the twin-screw extruder were 170–200 °C from the hopper to die.

The extrudates were dried and then compression molded in a hot press (XLB, Qingdao No. 3 Rubber Machine Company) at 10 MPa and 200 °C for 5 min, in order to obtain standard tensile and Izod impact bars.



Scheme 1 Processing of the melt blending via the lateral injection extrusion for PP/EPDM/nano-CaCO₃ composites

Scanning electron microscopy (SEM)

The extruded samples were cryogenically fractured in liquid nitrogen perpendicular to the flow direction. Then EPDM phase was preferentially etched in dimethylbenzene and the etched samples were carefully washed several times using fresh dimethylbenzene and then with acetone. The samples were dried in air at room temperature for 24 h and then coated with a thin layer of gold. Finally, the morphology was observed by a JSM-5900LV SEM at an accelerating voltage of 20 kV.

Transmission electron microscopy (TEM)

The morphologies of the ternary composites were characterized by transmission electron microscopy (TEM). Ultrathin sections for TEM (FEI-Tecnaï G2F20, USA) were cut using a cryo-ultramicrotome equipped (Leica-EM FC6, German) with a diamond knife. Samples were cooled below the glass transition of the polymer during cutting, and a speed of 1 mm/s was used to cut 50- to 100-nm-thick sections. Sections were then collected on 400-mesh copper grids, followed by staining with osmium tetroxide (OsO₄) to enhance contrast between the PP phase and EPDM phase. TEM was performed on a Philips CM 200 operating at 200 kV and images were recorded using a CCD camera.

Dynamic mechanical analysis (DMA)

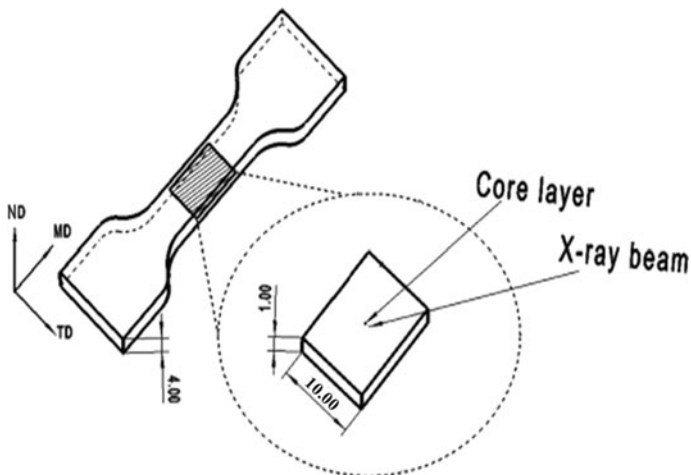
The dynamic mechanical analysis was carried out with a TA Q800 DMA. All the samples were measured in a stretching mode over the temperature range of -80 to 150 °C at a heating rate of 5 °C/min and at a frequency of 10 Hz. The samples were cut from the compression-molded specimen and the dimension was 35 mm \times 10 mm \times 4.2 mm.

Mechanical testing

The tensile modulus was performed at 23 °C according to ASTM D-638 at a cross-head speed of 5 mm min⁻¹. The notched impact test was carried out at 23 ± 2 °C in an UJ-40 impact tester according to ASTM D256 on the standard sized rectangular bars having a 45° V-notch (depth of 2 mm). A minimum of five specimens were tested and the average result was reported.

Two-dimensional wide-angle X-ray diffraction (2D-WAXD)

To characterize the crystalline structure in the width direction, two-dimensional wide-angle X-ray diffraction (2D-WAXD) was used. We started with a 10.0-mm wide and 4.0-mm-thick dumbbell tensile bar and machined away all of the tensile bar except for a 1.0-mm-thick piece (the 10.0 mm width remains unchanged) in the middle of the thickness, as shown in Scheme 2. The position of the sample obtained is located in the middle of the bar. The direction normal to MD–TD (the molding direction–transverse direction) plane was defined as ND. The X-ray beam with 1.0 mm width was perpendicular to the MD–TD plane, focusing on the core layer of the specimen. The measurements were carried on the synchrotron light source (wavelength $\lambda = 0.14809$ nm) with the MarCCD as the detector at National Synchrotron Radiation Laboratory, Hefei, China. The scattered intensities were registered in the range of scattering angles 2θ from 11° to 22.5°.



Scheme 2 Schematic diagram of the positions of the samples for WAXS measurement: *MD* the molding direction (i.e., flow direction), *TD* the transverse direction, *ND* the direction normal to the MD–TD plane

Results and discussion

Phase morphology

On the basis of the theories of interfacial tension and entropy penalty [24], CaCO_3 particles are predicted to be selectively distributed in the PP phase in the PP/EPDM blend, and this prediction is confirmed by TEM and SEM observations [32]. The distribution of nano- CaCO_3 varying with the initial mixing states is observed by the SEM photographs of the PP/EPDM/ CaCO_3 composite shown in Fig. 1. Apparently, PP is served as the continuous phase, while the spherical domains and the bright smaller particles belong to EPDM phase and nano- CaCO_3 particles, respectively. It is seen that nano- CaCO_3 particles and EPDM particles are separately distributed in the PP matrix in the solid blending composites, where smooth no nanoparticles are observed at the interface between PP and EPDM (Fig. 1a), similar to PP/EPDM blend (Fig. 1d). Besides, in the solid blending composite there are large aggregates of CaCO_3 particles in PP phase, resembling PP/ CaCO_3 composite (Fig. 1e). In the process of producing master batch composite, nano- CaCO_3 particles are blended with EPDM first, so that nano- CaCO_3 particles were well dispersed in EPDM phase. Compared to the solid blending composite, fewer nano- CaCO_3 particles are dispersed in PP phase, while more CaCO_3 particles exist at the interface between PP and EPDM in the master batch composite, as shown in Fig. 1b. Interestingly, abundant CaCO_3 particles are concentrated at the interface between EPDM and matrix phase or around EPDM dispersed phase in the melt blending composites in Fig. 1c. It is worth noting that the morphology of PP/EPDM/nano- CaCO_3 composites with 4 phr nano- CaCO_3 is similar and not shown here.

The diverse morphologies of the PP/EPDM/nano- CaCO_3 composites are attributed to the initial mixing state and migration of CaCO_3 particles between the two polymer components. In the solid blending composite, CaCO_3 particles and polymer pellets were compounded together. PP pellets were melted first, then the CaCO_3 particles were directly dispersed in the melt PP without migration; meanwhile, the breaking up of EPDM droplets and the aggregating of CaCO_3 particles occurred independently, thus large CaCO_3 aggregates were formed in the PP matrix. The sketch of the CaCO_3 distribution in the PP/EPDM/nano- CaCO_3 composite with the solid blending is shown in Fig. 2a. When EPDM/ CaCO_3 were both present in master batch, CaCO_3 particles were well dispersed in EPDM phase firstly. The migration of CaCO_3 from EPDM dispersed phase to PP matrix occurred spontaneously in the later extrusion. The migration could be divided into two stages. At first, CaCO_3 particles migrated from EPDM phase to interface between two polymers due to the breaking of EPDM droplets caused by shear during the extrusion processing, and subsequently moved from the interface to matrix. It implied that CaCO_3 particles would reside at the interface for a certain period of time because the EPDM molecules absorbed on the CaCO_3 surface must desorb progressively to be replaced by the PP chains, which prevented the coalescence of EPDM droplets and the aggregation of CaCO_3 particles. Therefore, well-dispersed CaCO_3 particles in the PP matrix were certainly formed as shown in Fig. 2b. During the melt blending, CaCO_3 particles were also first well dispersed in EPDM phase,

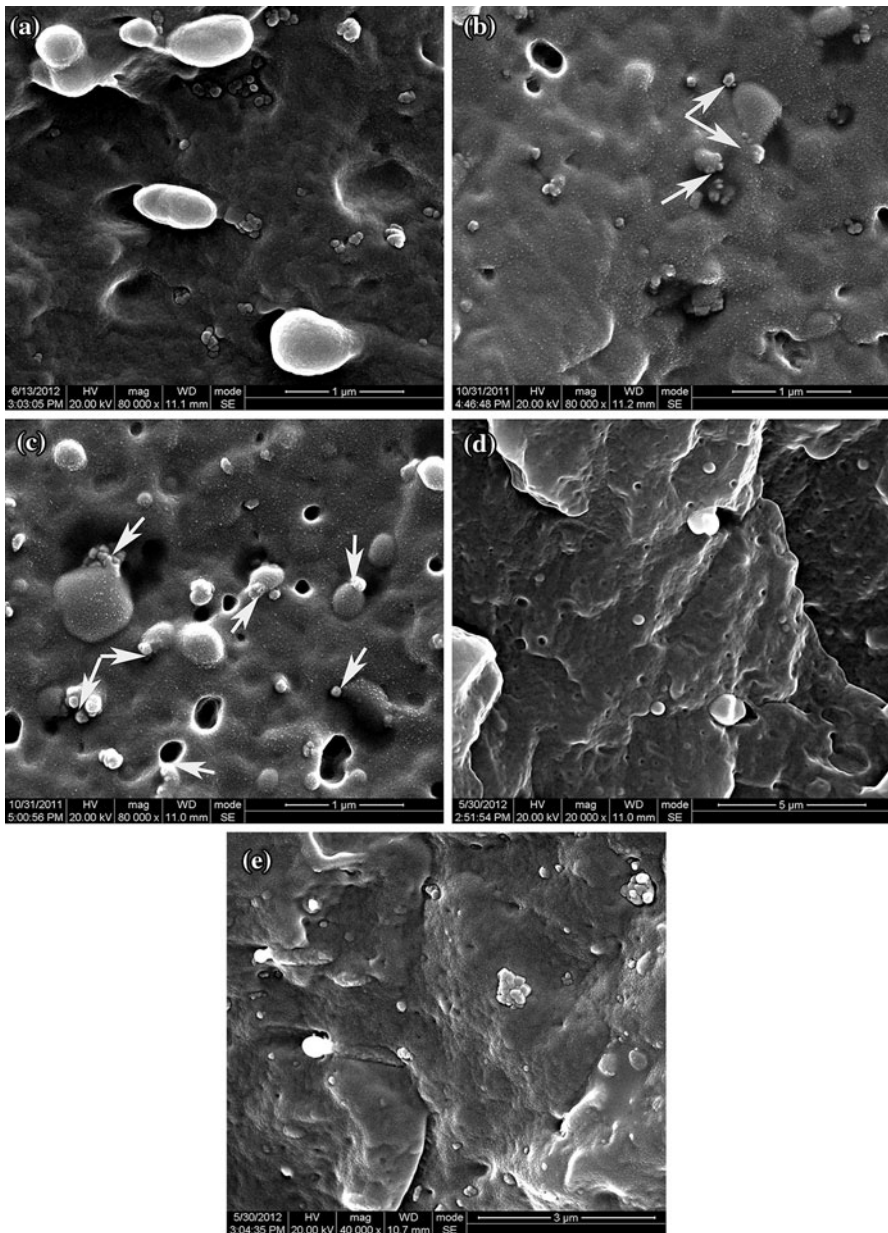


Fig. 1 The SEM photographs of PP/EPDM/nano-CaCO₃ (80/20/6) composites with different initial mixing states: **a** solid blending $\times 80,000$, **b** master batch blending $\times 80,000$, **c** melt blending $\times 80,000$, and PP/EPDM 80/20, $\times 20,000$ (**d**), PP/CaCO₃ 80/6, $\times 40,000$ (**e**) as a comparison

and then the EPDM/nano-CaCO₃ compounds melt was injected to the PP melt, where the migration of nano-CaCO₃ particles from the higher melt viscosity phase (EPDM) to the lower melt viscosity phase (PP) occurred, which is believed to be

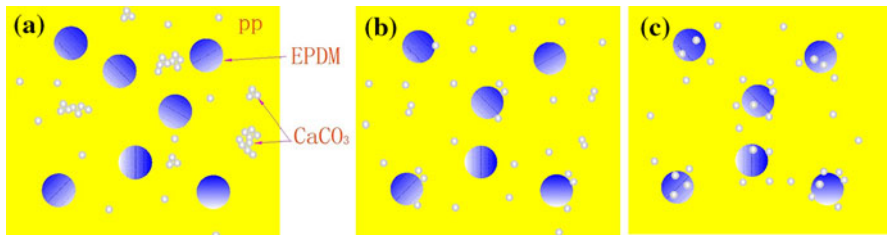


Fig. 2 Sketch of the distribution of nano- CaCO_3 and EPDM in PP with different initial mixing states: **a** solid blending, **b** master batch blending, **c** melt blending

caused by the minimization of the dissipative energy [30]. When the EPDM melt was just injected from lateral port to mix with the PP phase, the elastomer presented instantaneous local high concentration which reduced the opportunity for collision of CaCO_3 particles and PP chains. With further mixing, the local concentration of EPDM droplets became thin, then the locally continuous EPDM droplets broke up to form the dispersed particles after further strong shear. Furthermore, there was lack of time for the complete migration of CaCO_3 particles from EPDM phase to the PP phase. Therefore, considerable CaCO_3 particles were reserved in/around the EPDM phase, which is roughly depicted in Fig. 2c.

The microstructure of the melt blending composite was further characterized in different magnification by TEM, as shown in Fig. 3. The light color region represented PP matrix, and the gray domains and the dark particles were EPDM dispersed phase and nano- CaCO_3 particles, respectively. Clearly well-dispersed CaCO_3 particles concentrated around EPDM dispersed phase, and at the interface between EPDM and PP phase in the melt blending composites. This special morphology would bring some special properties to the melt blending composites, which may be different from the composites in other initial mixing states.

Mechanical properties

Figure 4a displays the Young's modulus of PP/EPDM/ CaCO_3 composites in different initial mixing states. A slight enhancement in the Young's modulus was observed after the addition of CaCO_3 , whereas a significant drop in the Young's modulus was generally expected after mixing with EPDM, compared to pure PP. For the solid blending composite and master batch blending composite, the introduction of CaCO_3 in the small concentration (4 phr) does not significantly alter the stiffness of PP/EPDM blend, while a slight reduction was observed in blends with the higher CaCO_3 concentration (6 phr). The slight reduction in stiffness was also observed in many other studies [13, 36]. The impact strength of PP was greatly improved by blending with 20 wt% EPDM and was limitedly enhanced by only adding nano- CaCO_3 . However, the impact strength of the ternary composites has been gradually improved by the incorporation of nano- CaCO_3 into PP/EPDM blend. For the three initial mixing states of the components, the melt blending composites endows the highest impact strength for both contents of nano- CaCO_3 (4 and 6 phr), i.e., 24.96 and 21.97 kJ/m^2 for 4 and 6 phr, respectively, which is remarkably

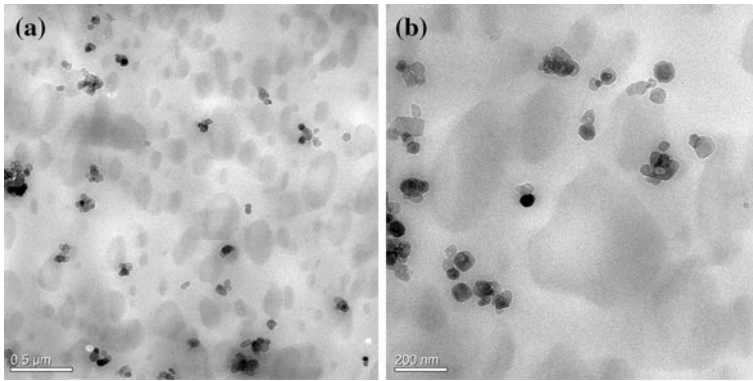


Fig. 3 TEM photographs showing the phase morphology appearing in the PP/EPDM/nano-CaCO₃ (80/20/6) composite for melt blending: **a** ×10,000, **b** ×80,000

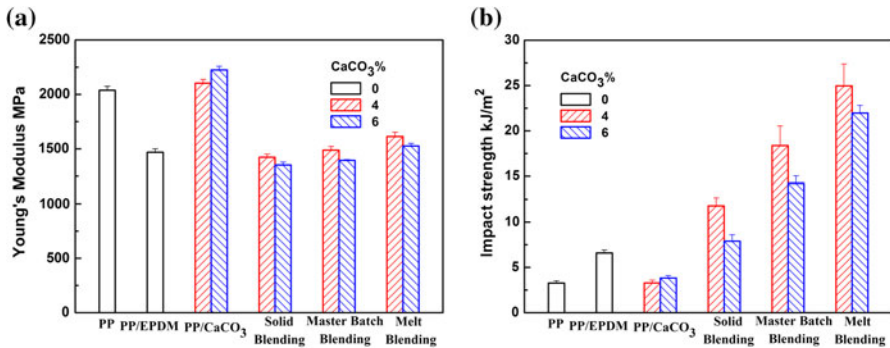


Fig. 4 The tensile modulus (a) and the impact strength (b) of PP/EPDM/nano-CaCO₃ blends in different initial mixing states of the compositions

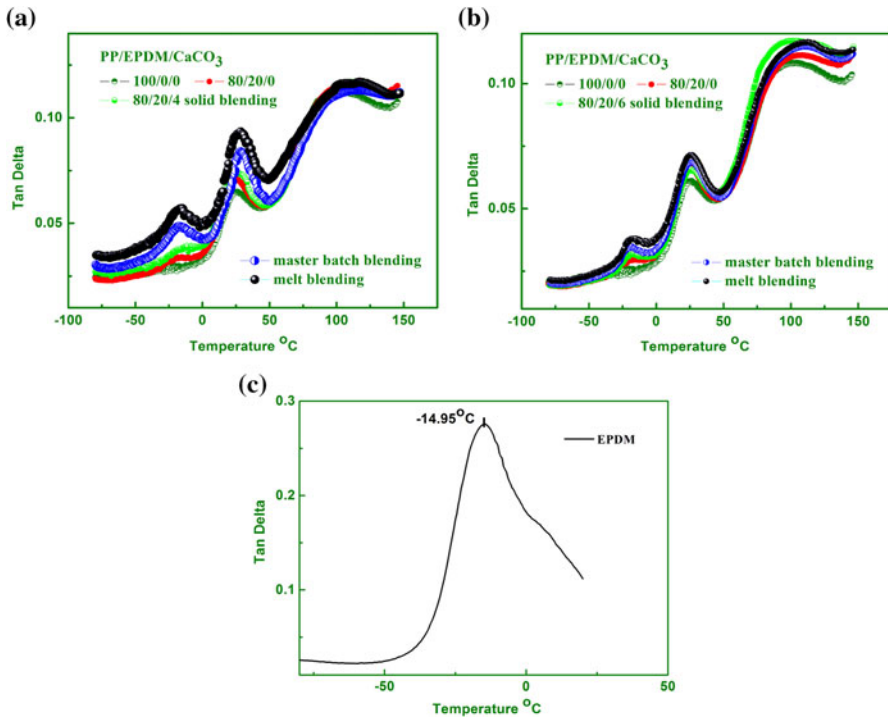
improved by 280 and 234 %, compared to PP/EPDM blend. The impact strength of the composites in master batch significantly surpasses that of the solid blending composites by 55.8 and 80.7 % for 4 and 6 phr nano-CaCO₃. Herein, it can be concluded that the melt blending composite with 4 phr nano-CaCO₃ achieved the simultaneous improvement of the stiffness and impact toughness, compared to PP/EPDM blend (Table 1).

Dynamic mechanical analysis

Figure 5 presents $\tan\delta$ for PP/EPDM/nano-CaCO₃ composites with various content of nano-CaCO₃. Two $\tan\delta$ peaks corresponding to the glass transition temperatures (T_g) of PP and EPDM can be observed. The glass transition temperatures and the peak intensity of the blend are listed in Table 2. It is noted that the heating rate of 5 °C/min used here is faster than that in other studies [37, 38], which leads to higher glass transition temperatures of PP and EPDM [39].

Table 1 Different initial mixing states of the components for PP/EPDM/CaCO₃ blend

Blending process	Components		
	PP	EPDM	CaCO ₃
Solid blending	Solid	Solid	Solid
Master batch blending	Solid	Master batch and solid	
Melt blending	Melt	Master batch and melt	

**Fig. 5** Loss factor of PP/EPDM/nano-CaCO₃ composites with various content of nano-CaCO₃: **a** 80/20/4, **b** 80/20/6, and of EPDM **(c)** as a comparison

The T_g of EPDM in PP/EPDM (80/20) blend (-18.32 °C) decreases for almost 3 °C compared with that of pure EPDM (-15 °C) (Fig. 5c). However, all the ternary composites with nano-CaCO₃ promote the T_g of EPDM, which signifies the influence of stiff nano-CaCO₃. Among the ternary composites with 4 or 6 phr nano-CaCO₃ varies with the initial mixing states, the melt blending composites exhibit the highest T_g of EPDM and the solid blending composites possess the lowest. The T_g of EPDM in the solid blending composites with both contents is almost constant, -18 °C, indicating that nano-CaCO₃ particles are rarely dispersed in EPDM phase [23, 40]. The further improved T_g of EPDM in the master batch blending composites implies nano-CaCO₃ particles are mainly present in the EPDM phase. In

Table 2 Glass transition temperatures and peak intensity of PP/EPDM/nano-CaCO₃ composites

PP/EPDM/CaCO ₃	<i>T_g</i> (EPDM) °C	<i>T_g</i> (PP) °C	<i>I_B</i> × 10 ²	<i>A</i>
100/0/0		26.79		
0/100/0	−15			
80/20/0	−18.32	25.1	10.5	
80/20/4 solid blending	−17.99	24.21	11.3	5.58
Master batch blending	−16.88	28.72	13.3	6.08
Melt blending	−14.3	28.44	15.1	7.08
80/20/6 solid blending	−18.71	26.03	9.7	4.63
Master batch blending	−18.32	26.42	10.4	4.79
Melt blending	−17.4	26.68	11.0	5.13

comparison to other composites, a greater shift of *T_g* of EPDM to a higher temperature is observed for the melt blending composites, because more nano-CaCO₃ particles restraining the mobility of EPDM chains are almost dispersed in EPDM phase or at the interphase between EPDM and PP phase [24]. These results are in accordance with the aforementioned SEM observation. Li et al. [37] presented similar results for the high-density polyethylene (HDPE)/scrap rubber powder (SRP)/POE composite, where the encapsulation of the filler by elastomer led to a higher *T_g* of elastomer than the separately dispersed type.

The *T_g* peaks of PP in the PP/EPDM/nano-CaCO₃ composite in solid blending are nearly the same as that in the PP/EPDM blend. While The *T_g* of PP for the other two composites increase by about 3 °C on blending with 4 phr nano-CaCO₃, but basically remains unchanged on blending with 6 phr nano-CaCO₃.

Correlation of the impact strength with dynamic mechanical properties

DMA has been proved to be a useful tool in estimating the fracture toughness of polymer and its blends [38, 41]. *I_B*, the relaxation intensity or viscoelastic energy dissipation of the blends, can be calculated from the peak intensity by Eq. (1):

$$I_B = I_P + I_E \quad (1)$$

where *I_P* and *I_E* are the intensity of tanδ peak of PP and EPDM component, respectively. Figure 6 shows *I_B* dependency of impact strength for PP/EPDM (80/20)/nano-CaCO₃ composite with different contents of nano-CaCO₃. It can be found that the impact strength of the PP/EPDM/nano-CaCO₃ composites with the same composition is proportional to *I_B* of the blend, suggesting that the increase of relaxation intensity or viscoelastic energy dissipation of the composites, is accompanied by an increase of impact strength [42]. An increase in slope with the increasing content of nano-CaCO₃ was further exhibited for the PP/EPDM/nano-CaCO₃ composites, which is related to the degree of the increase for the impact strength.

The area under the loss peak (*A*) is corresponding to total energy dissipation because of viscoelastic relaxation of both PP and EPDM. Plots of impact strength

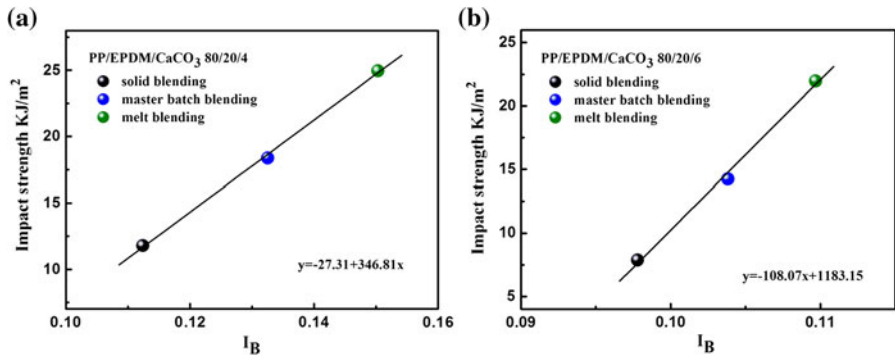


Fig. 6 I_B dependency of impact strength for PP/EPDM (80/20)/nano-CaCO₃ composites with different content of nano-CaCO₃: **a** 4 phr, **b** 6 phr

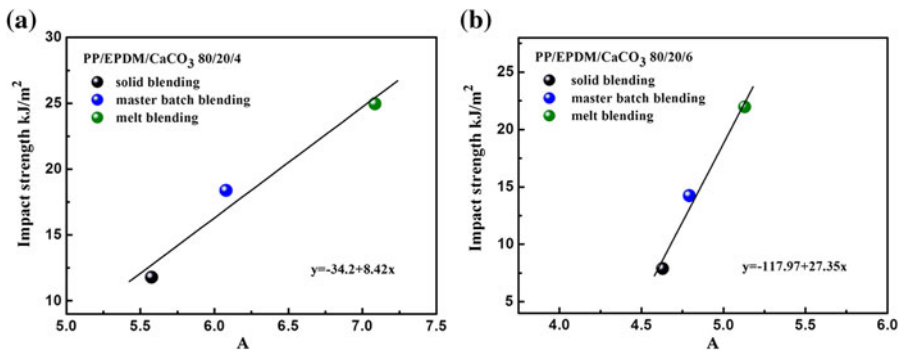


Fig. 7 A dependency of impact strength for PP/EPDM (80/20)/nano-CaCO₃ composites with different content nano-CaCO₃: **a** 4 phr, **b** 6 phr

versus A for the PP/EPDM/nano-CaCO₃ composites in different initial mixing states are shown in Fig. 7. From Fig. 7, it is seen that with the increase of A , the impact strength also increases. A linear relationship between the impact strength and A was also observed in PP/EPDM/nano-CaCO₃ composites in different initial mixing states. This suggests that the viscoelastic energy dissipation is quite significant in the impact fracture of these composites. A larger slope was observed for PP/EPDM/nano-CaCO₃ composite with 6 phr nano-CaCO₃, compared to that with 4 phr nano-CaCO₃. Actually, the larger slope means the greater extent of enhancement for the impact strength.

Toughing mechanism

Since the molecular orientation will play a role in determining the mechanical properties, 2D-WAXS experiments were performed to inspect the orientation. Figure 8 shows the selected 2D-WAXS patterns of PP/EPDM/nano-CaCO₃ (80/20/6) composites in different initial mixing states in core layer parallel to the melt shear

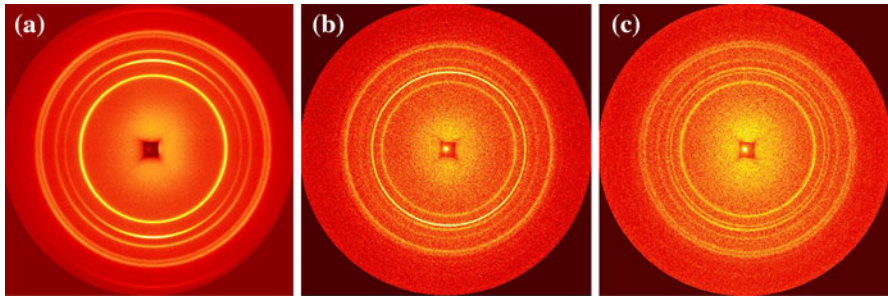


Fig. 8 Selected 2D-WAXS patterns of neat PP (a) and PP/EPDM/nano-CaCO₃ composites in different initial mixing states: **b** solid blending, **c** melt blending

flow direction. No distinct oriented structure is evident in any ternary composite in different initial mixing states as well as in binary blend and pure PP. The effect of molecular orientation on the mechanical properties [43] can be ignored in the ternary composites. In other words, the enhanced mechanical properties for melt blending composite are not ascribed to the orientation of PP in the composites.

In order to figure out the reason for the improvement of the mechanical properties, SEM photographs of the impact-fractured surface of PP/EPDM/nano-CaCO₃ (80/20/6) composites in different initial mixing states were investigated in Fig. 9. A typical brittle failure surface is present in PP (Fig. 9a). Many microvoids and a relatively flat surface are observed in PP/EPDM blend (Fig. 9b) and the solid blending composites (Fig. 9c), without any apparent plastic deformation. However, abundant fibril globules in a range of 3.5–20 μm can be seen in the master batch blending composites as white circles shown in Fig. 9d. Intriguingly, many larger fibril globules as white circles shown in Fig. 9e and abundant cavities and elongated microfibrils around the dispersed particles, and further obvious plastic deformation in PP matrix were displayed in the melt blending composite (Fig. 9f). As is extensively described in the literature, cavitation is an important energy dissipating deformation way in the rubber-toughened thermoplastic materials [41, 44, 45]. Cavities can occur either by internal cavitation or debonding [46–48].

In Fig. 10, the small cavities in gray pointed out by arrows perhaps occurred by internal cavitation of EPDM particles, which were insufficient in our system but dominant in PLA/EBA-GMA/EMAA-Zn blend [45] and PA6/EPM-g-MA blend [49]. However, the large cavities prevailed, which were initiated by the debonding of EPDM particles from PP matrix at the interface. Therefore, interfacial debonding was considered as the predominant toughening mechanism rather than internal cavitation of the dispersed particles followed by the matrix plastic deformation. The formation of microfibrils may be due to the interfacial activity of nano-CaCO₃ concentrating around EPDM dispersed phase as a compatibilizer for PP/EPDM blend, which increases adhesive strength between the dispersed and the matrix phases [27]. It has been reported that, a suitable level of interfacial strength was needed to achieve optimal impact toughness in polymer blends [50]. Low interfacial adhesion easily caused premature interfacial failure and hence rapid and catastrophic crack propagation, such as the debonding of rigid inorganic filler in

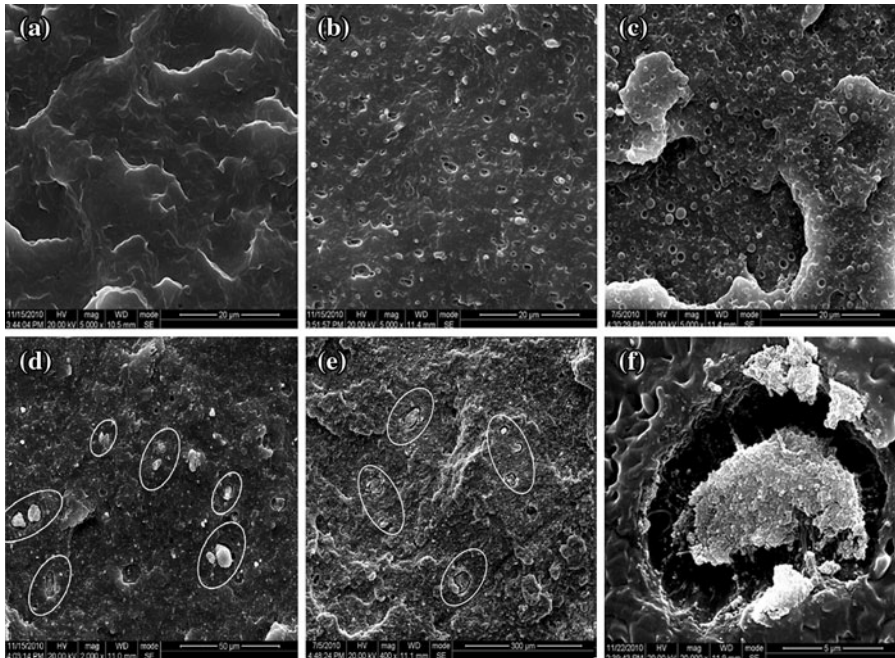


Fig. 9 The SEM photographs of impact-fractured surface for PP/EPDM/CaCO₃ (80/20/6) composites in different initial mixing states: **a** PP $\times 5,000$, **b** PP/EPDM 80/20, $\times 5,000$, **c** solid blending $\times 5,000$, **d** master batch blending $\times 2,000$, **e** melt blending $\times 400$ and **f** melt blending $\times 20,000$

the CaCO₃/nylon-6 blends with negligible interfacial adhesion [51], whereas very strong adhesion was unfavorable for debonding and also delayed the occurrence of matrix yielding [52]. Charoensirisomboon et al. [53] and Na et al. [54] put forward that the toughness improvement was attributed to the fibrillation of dispersed particles in PA/PSU and PA6/PVDF blends with suitable interfacial adhesion. And this argument is somewhat consistent with the cold drawing concept presented in the brittle organic particles toughened ductile polymers [55, 56]. Hence, the cavitation initiated by the debonding of EPDM particles and the fibrillation due to suitable interfacial adhesion could dissipate energy to a large extent and result in the toughness enhancement for the melt blending composite.

A schematic deformation process for the melt blending composite during the impact testing is explicitly described below. Owing to the different elastic properties and the distinguishing Poisson's ratio from the matrix, the EPDM particles first act as stress concentration under load, and then are separated from the matrix at their interphase. Resulting from the nano-CaCO₃ dispersed in EPDM phase and at the interphase between EPDM phase and matrix, EPDM particles have better compatibility with the PP matrix. Therefore, the matrix is stretched to form fibrils and abundant large cavities are formed at the interface between PP and EPDM phase when the separation process occurs. Substantive energy can be absorbed during the fibrillation process. In this case, nano-CaCO₃ particles play two effective roles

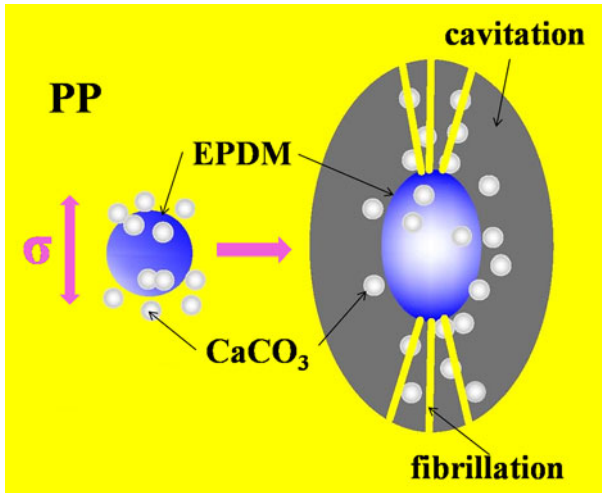


Fig. 10 A schematic representation of deformation process for the melt blending composite during the impact testing

during the impact fracture process: (1) act as an active compatibilizer [27]; (2) decrease the interparticle distance and cause the overlapping of the stress field between EPDM and nano- CaCO_3 particles [24].

Conclusion

The phase morphology and mechanical properties of the PP/EPDM/nano- CaCO_3 composites with different initial mixing states of the components (solid, master batch and melt) were investigated. The nano- CaCO_3 distribution in the ternary composites was strongly influenced by the initial mixing states, which further affected the mechanical performance of the ternary composites. When the mixing components were all melted at the beginning of blending (melt blending composite), abundant well-dispersed nano- CaCO_3 particles concentrating around EPDM phase were achieved, totally different from the solid blending composite with nano- CaCO_3 particles dispersing in the PP matrix. Therefore, the melt blending composites maintained pronouncedly improved impact strength and higher dynamic mechanical loss, compared with the other two composites. The morphological observation on the impact-fractured surface suggested that the significantly enhanced impact strength for melt blending composite was predominantly ascribed to the cavitation initiated by the debonding and the fibrillation present at interface, rather than the orientation of PP matrix.

Acknowledgments The authors gratefully acknowledge the financial support from the National Natural Science Foundation of China (Contract No. 51273219). Thanks go to Prof. Guo-Qiang Pan and Mr. Li-Hui Wu from National Synchrotron Radiation Laboratory (China) for synchrotron WAXS measurements.

References

1. Zhang Y, Zhang XF, Peng ZL (2000) Dynamically vulcanized nitrile rubber/polyoxymethylene thermoplastic elastomers. *J Appl Polym Sci* 77:2641–2645
2. Dariusz M, Bielinski L, Slusarski (1997) Some aspects of isotactic polypropylene crystallization in an ethylene–propylene–diene rubber matrix. *Polym Int* 44:161
3. Kalay G, Bevis MJ (1997) The effect of shear controlled orientation in injection moulding on the mechanical properties of an aliphatic polyketone. *J Polym Sci Part B-Polym Phys* 35:415–430
4. van der Wal A, Nijhof R, Gaymans RJ (1999) Polypropylene–rubber blends: 2. The effect of the rubber content on the deformation and impact behaviour. *Polymer* 40:6031–6044
5. Galli P, Vecellio G (2001) Technology: driving force behind innovation and growth of polyolefins. *Prog Polym Sci* 26:1287–1336
6. Bucknall CB, Soares VLP, Yang HH, Zhang XC (1996) *Macromol Symp* 101:265–271
7. Karnani R, Krishnan M, Narayan R (1997) Biofiber-reinforced polypropylene composites. *Polym Eng Sci* 37:476–483
8. Thio YS, Argon AS, Cohen RE, Weinberg M (2002) Toughening of isotactic polypropylene with CaCO₃ particles. *Polymer* 43:3661–3674
9. Chen HB, Karger-Kocsis J, Wu JS, Varga J (2002) Fracture toughness of alpha- and beta-phase polypropylene homopolymers and random- and block-copolymers. *Polymer* 43:6505–6514
10. Varga J, Menyhard A (2007) Effect of solubility and nucleating duality of N,N'-dicyclohexyl-2,6-naphthalenedicarboxamide on the supermolecular structure of isotactic polypropylene. *Macromolecules* 40:2422–2431
11. Dasari A, Zhang QX, Yu ZZ, Mai YW (2010) Toughening Polypropylene and Its Nanocomposites with Submicrometer Voids. *Macromolecules* 43:5734–5739
12. Shah D, Maiti P, Gunn E, Schmidt DF, Jiang DD, Batt CA, Giannelis ER (2004) Dramatic enhancements in toughness of polyvinylidene fluoride nanocomposites via nanoclay-directed crystal structure and morphology. *Adv Mater* 16:1173
13. Zuiderduin WCJ, Westzaan C, Huetink J, Gaymans RJ (2003) Toughening of polypropylene with calcium carbonate particles. *Polymer* 44:261–275
14. Chen YH, Zhong GJ, Wang Y, Li ZM, Li L (2009) Unusual Tuning of Mechanical Properties of Isotactic Polypropylene Using Counteraction of Shear Flow and beta-Nucleating Agent on beta-Form Nucleation. *Macromolecules* 42:4343–4348
15. Amash A, Zugenmaier P (1997) Dynamic mechanical investigations on drawn samples of isotactic polypropylene/EPM–Rubber blend. *J Polym Sci Part B Polym Phys* 35:1439
16. Schrauwen BAG, Breemen LCAV, Spoelstra AB, Govaert LE, Peters GWM, Meijer HEH (2004) Structure, Deformation, and Failure of Flow-Oriented Semicrystalline Polymers. *Macromolecules* 37:8618–8633
17. Lovinger AJ, Chua JO, Gryte CC (1976) An apparatus for in situ microscopy of zone solidifying polymers. *J Phys E (Sci Instrum)* 9:927–929
18. Ma CG, Rong MZ, Zhang MQ, Friedrich K (2005) Irradiation-induced surface graft polymerization onto calcium carbonate nanoparticles and its toughening effects on polypropylene composites. *Polym Eng Sci* 45:529–538
19. Bucknall CB, Paul DR (2009) Notched impact behavior of polymer blends: Part 1: New model for particle size dependence. *Polymer* 50:5539–5548
20. Sahnoune F, Cuesta JML, Crespy A (2003) Improvement of the mechanical properties of an HDPE/PS blend by compatibilization and incorporation of CaCO₃. *Polym Eng Sci* 43:647–660
21. Shanks RA, Long Y (1997) Brittle-tough transition of polypropylene-elastomer-filler hybrids. *Polym Netw Blends* 7:87–92
22. Fisher I, Siegmann A, Narkis M (2002) The effect of interface characteristics on the morphology, rheology and thermal behavior of three-component polymer alloys. *Polym Compos* 23:34–48
23. Yang H, Zhang Q, Guo M, Wang C, Du R, Fu Q (2006) Study on the phase structures and toughening mechanism in PP/EPDM/SiO₂ ternary composites. *Polymer* 47:2106–2115
24. Yang H, Zhang X, Qu C, Li B, Zhang L, Zhang Q, Fu Q (2007) Largely improved toughness of PP/EPDM blends by adding nano-SiO₂ particles. *Polymer* 48:860–869
25. Ma CG, Mai YL, Rong MZ, Ruan WH, Zhang MQ (2007) Phase structure and mechanical properties of ternary polypropylene/elastomer/nano-CaCO₃ composites. *Compos Sci Technol* 67:2997–3005

26. Liu Y, Kontopoulou M (2006) The structure and physical properties of polypropylene and thermoplastic olefin nanocomposites containing nanosilica. *Polymer* 47:7731–7739
27. Sinha Ray S, Pouliot S, Bousmina M, Utracki LA (2004) Role of organically modified layered silicate as an active interfacial modifier in immiscible polystyrene/polypropylene blends. *Polymer* 45:8403–8413
28. Zhang Q, Yang H, Fu Q (2004) Kinetics-controlled compatibilization of immiscible polypropylene/polystyrene blends using nano-SiO₂ particles. *Polymer* 45:1913–1922
29. Lee HS, Fasulo PD, Rodgers WR, Paul DR (2005) TPO based nanocomposites. Part 1. Morphology and mechanical properties. *Polymer* 46:11673–11689
30. Guo HF, Packirisamy S, Gvozdic NV, Meier DJ (1997) Prediction and manipulation of the phase morphologies of multiphase polymer blends. I. Ternary systems. *Polymer* 38:785–794
31. Dasari A, Yu ZZ, Mai YW (2005) Effect of blending sequence on microstructure of ternary nanocomposites. *Polymer* 46:5986–5991
32. Wang X, Xu KJ, Xu XB, Park SJ, Kim S (2009) Selective particle distribution and mechanical properties of nano-CaCO₃/ethylene-propylene-diene terpolymer/polypropylene composites with high content of nano-CaCO₃. *J Appl Polym Sci* 113:2485–2491
33. Gong L, Yin B, Li LP, Yang M-B (2012) Morphology and properties of PP/EPDM binary blends and PP/EPDM/nano-CaCO₃ ternary blends. *J Appl Polym Sci* 123:510–519
34. Gong L, Yin B, Li LP, Yang M-B (2011) The effects of different processing methods on the morphology and properties of PP/EPDM/Nano-CaCO₃ ternary blend. *J Macromol Sci B Phys* 50:806–820
35. Tao R, Liu ZY, Yang W, Yang MB (2008) Effect of dispersion condition of calcium carbonate on the crystallization and melting behavior of polypropylene/CaCO₃ nanocomposites. *Polym Plast Technol Eng* 47:490–495
36. Bartczak Z, Argon AS, Cohen RE, Weinberg M (1999) Toughness mechanism in semi-crystalline polymer blends: I. High-density polyethylene toughened with rubbers. *Polymer* 40:2331–2346
37. Li Y, Zhang Y, Zhang YX (2004) Morphology and mechanical properties of HDPE/SRP/elastomer composites: effect of elastomer polarity. *Polym Test* 23:83–90
38. Han L, Li X, Li Y, Huang T, Wang Y, Wu J, Xiang F (2010) Influence of annealing on microstructure and physical properties of isotactic polypropylene/calcium carbonate composites with beta-phase nucleating agent. *Mater Sci Eng Struct Mater Prop Microstruct Process* 527:3176–3185
39. Jain AK, Nagpal AK, Singhal R, Gupta NK (2000) Effect of dynamic crosslinking on impact strength and other mechanical properties of polypropylene/ethylene-propylene-diene rubber blends. *J Appl Polym Sci* 78:2089–2103
40. Tsagaropoulos G, Eisenberg A (1995) Dynamic mechanical study of the factors affecting the two glass transition behavior of filled polymers. Similarities and differences with random ionomers. *Macromolecules* 28:6067–6077
41. Narisawa I, Murayama T, Ogawa H (1982) Internal fracture of notched epoxy resins. *Polymer* 23:291–294
42. Jafari SH, Gupta AK (2000) Impact strength and dynamic mechanical properties correlation in elastomer-modified polypropylene. *J Appl Polym Sci* 78:962–971
43. Wang K, Wang C, Li J, Su J, Zhang Q, Du R, Fu Q (2007) Effects of clay on phase morphology and mechanical properties in polyamide 6/EPDM-g-MA/organoclay ternary nanocomposites. *Polymer* 48:2144–2154
44. Ishikawa M (1995) Stability of plastic deformation and toughness of polycarbonate blended with poly(acrylonitrile-butadiene-styrene) copolymer. *Polymer* 36:2203–2210
45. Liu H, Song W, Chen F, Guo L, Zhang J (2011) Interaction of microstructure and interfacial adhesion on impact performance of polylactide (PLA) ternary blends. *Macromolecules* 44:1513–1522
46. Borggreve RJM, Gaymans RJ, Eichenwald HM (1989) Influence of structure on voiding processes; toughening mechanism. *Polymer* 30:78–83
47. Sue HJ, Huang J, Yee AF (1992) Interfacial adhesion and toughening mechanisms in an alloy of polycarbonate/polyethylene. *Polymer* 33:4868–4871
48. Dompas D, Groeninckx G, Isogawa M, Hasegawa T, Kadokura M (1995) Cavitation versus debonding during deformation of rubber-modified poly(vinyl chloride). *Polymer* 36:437–441
49. Adriaensens P, Storme L, Carleer R, D'Haen J, Gelan J, Litvinov VM, Marissen R, Crevecoeur J (2002) NMR imaging study of stress-induced material response in rubber modified polyamide 6. *Macromolecules* 35:135–140

50. Wu JS, Mai YW, Yee AF (1994) Fracture toughness and fracture mechanisms of polybutylene-terephthalate/polycarbonate/impact-modifier blends. *J Mater Sci* 29:4510–4522
51. Wilbrink MWL, Argon AS, Cohen RE, Weinberg M (2001) Toughenability of Nylon-6 with CaCO_3 filler particles: new findings and general principles. *Polymer* 42:10155–10180
52. Liu Z, Zhu X, Wu L, Li Y, Qi Z, Choy C, Wang F (2001) Effects of interfacial adhesion on the rubber toughening of poly(vinyl chloride) Part 1. Impact tests. *Polymer* 42:737–746
53. Charoensirisomboon P, Chiba T, Torikai K, Saito H, Ougizawa T, Inoue T, Weber M (1999) Morphology-interface-toughness relationship in polyamide/polysulfone blends by reactive processing. *Polymer* 40:6965–6975
54. Na B, Xu W, Lv R, Li Z, Tian N, Zou S (2010) Toughening of nylon-6 by semicrystalline poly(vinylidene fluoride): role of phase transformation and fibrillation of dispersed particles. *Macromolecules* 43:3911–3915
55. Angola JC, Fujita Y, Sakai T, Inoue T (1988) Compatibilizer-aided toughening in polymer blends consisting of brittle polymer particles dispersed in a ductile polymer matrix. *J Polym Sci Part B Polym Phys* 26:807–816
56. Ohta T, Kurauchi T (1984) Energy absorption in blends of polycarbonate with ABS and SAN. *J Mater Sci* 19:1699–1709